NANO LETTERS

Letter

pubs.acs.org/NanoLett

Large Conductance Switching in a Single-Molecule Device through Room Temperature Spin-Dependent Transport

Albert C. Aragonès,[†,‡,§] Daniel Aravena,[∥,⊥] Jorge I. Cerdá,[#] Zulema Acís-Castillo,[▽] Haipeng Li,[○] José Antonio Real,[▽] Fausto Sanz,[†,‡,§] Josh Hihath,[*,○] Eliseo Ruiz,[*,∥] and Ismael Díez-Pérez[*,†,‡,§]

[†]Departament de Química Física, Universitat de Barcelona, Martí i Franquès 1, 08028 Barcelona, Spain

[‡]Institute for Bioengineering of Catalonia (IBEC), Baldiri Reixac 15-21, 08028 Barcelona, Spain

[§]Centro Investigación Biomédica en Red (CIBER-BBN), Campus Río Ebro-Edificio I+D, Poeta Mariano Esquillor s/n, 50018 Zaragoza, Spain

[∥]Departament de Química Inorgànica and Institut de Química Teòrica i Computacional, Universitat de Barcelona, Diagonal 645, 08028 Barcelona, Spain

[⊥]Departamento de Química de los Materiales, Facultad de Química y Biología, Universidad de Santiago de Chile (USACH), Casilla 40, Correo 33, Santiago, Chile

[#]Instituto de Ciencia de Materiales de Madrid, CSIC, Cantoblanco, 28049 Madrid, Spain

[▽]Institut de Ciència Molecular (ICMol), Universitat de València, 46980 Paterna, València, Spain

[○]Department of Electrical and Computing Engineering, University of California-Davis, 2064 Kemper Hall, Davis, California 95616, United States

S *Supporting Information*

ABSTRACT: Controlling the spin of electrons in nanoscale electronic devices is one of the most promising topics aiming at developing devices with rapid and high density information storage capabilities. The interface magnetism or *spinterface* resulting from the interaction between a magnetic molecule and a metal surface, or *vice versa*, has become a key ingredient in creating nanoscale molecular devices with novel functionalities. Here, we present a single-molecule wire that displays large (>10000%) conductance switching by controlling the spin-dependent transport under ambient conditions (room temperature in a liquid cell). The molecular wire is built by trapping individual spin crossover Fe^{II} complexes between one Au electrode and one ferromagnetic Ni electrode in an organic liquid medium. Large changes in the single-molecule conductance (>100-fold) are measured when the electrons flow from the Au electrode to either an α-up or a β-down spin-polarized Ni electrode. Our calculations show that the current flowing through such an interface appears to be strongly spin-polarized, thus resulting in the observed switching of the single-molecule wire conductance. The observation of such a high spin-dependent conductance switching in a single-molecule wire opens up a new door for the design and control of spin-polarized transport in nanoscale molecular devices at room temperature.

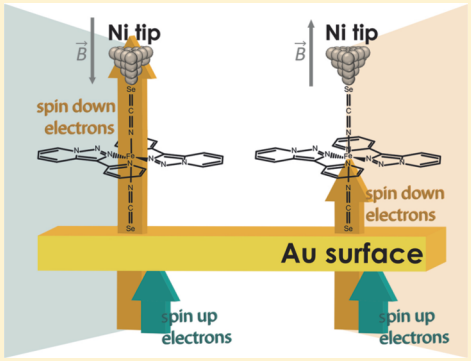

KEYWORDS: *Single-molecule junctions, spin-crossover complexes, magnetoresistance, STM break-junction, density functional calculations, spinterface, spin orbit coupling*

Controlling the spin of electrons has become one of the major challenges in the emerging field of Spintronics.[1,2] Electron spin offers an attractive extra degree of freedom, beyond the electron charge, which opens up a range of possibilities in the future design of electronic devices with new functionalities and larger bandwidths.[3] To fulfill today's technological needs, miniaturization is a requirement that must be pursued in the field of Spintronics, just as it has been in conventional electronics. Single-molecule devices promise to function both as a test-bench for fundamental studies in Spintronics and as a means to explore new routes for the design of organic, nanoscale, spin devices.[4] Spin-polarized scanning tunneling microscopy (SP-STM) has brought with it an extended realm of fundamental knowledge of the spin-dependent electronic structure of single magnetic molecules adsorbed on a metallic substrate.[5,6] SP-STM profits from the injection of spin-polarized currents into the STM junction to achieve spin mapping at subangstrom spatial resolutions.[7] Such experiments have allowed the visualization of a variety of hybridized spin-polarized states between a molecule and a

Received: September 4, 2015
Revised: November 13, 2015

DOI: 10.1021/acs.nanolett.5b03571
Nano Lett. XXXX, XXX, XXX−XXX

metal surface, giving rise to interfacial magnetism.[5,6,8−12] In this Letter, we explore this molecule−metal interfacial magnetism to design a new quantum nanoscale device that exploits the spin information.

A few examples of single-molecule spintronic devices have been presented,[13−15] and most that have, have resulted from the development of single-molecule transport approaches using nonmagnetic systems. Individual transition metal complexes displaying high-spin electronic configurations have been trapped between two nonmagnetic metal beads at low temperatures and the transport properties characterized at the single-molecule level.[16−18] In order to add spin-dependent functionalities to such single-molecule wires, magnetic Ni beads have been introduced into a junction formed with diamagnetic molecules,[5,19,20] resulting in observed changes in the single-molecule magnetoresistance. These results demonstrate the potential of nanoscale spin-selective transport, the performance of which might reach device application requirements by introducing metal complexes with much higher spin−orbit coupling.[21] Examples of this possibility include the characterization of magnetoresistive supramolecular nanoscale devices based on terbium^{III} complexes resulting in a number of spin functionalities such as spin valves,[22] spin transistors,[23] or spin resonators.[24] Such phtalocyaninate Tb^{III} molecules have become a reference in the metal/molecule interface studies, either with gold[25] or magnetic nickel surfaces.[26]

The fundamental studies mentioned above were performed far from practical operating conditions, such as ultrahigh vacuum (UHV) and low temperatures. However, room-temperature, spin-dependent transport has also been demonstrated through chiral structures such as DNA in a nanoscale device.[27] The mechanism has been well described for self-assembled monolayers (SAMs) as a combined effect of spin−orbit interaction in the chiral molecular structure[28,29] and the induced Au−S bond magnetization at the molecule−metal interface.[30−32] The latter effect has been experimentally observed on both gold surfaces and nanoparticles modified with thiolated molecules.[33,34] Although still under discussion, it originates in an amplification of the surface Rashba spin splitting at the bare metal surface[35] by the highly polarized metal-S bond.[30] Extensive theoretical studies support a spin-filter effect based on such interfacial Rashba effect.[36,37]

Spin crossover (SCO) complexes, most of them Fe^{II} complexes, have remarkable magnetic properties based on ground-state spin switching (for Fe^{II} systems, between the diamagnetic $S = 0$ low-spin $t_{2g}^6e_g^0$ and paramagnetic $S = 2$ high-spin $t_{2g}^4e_g^2$ electron configurations) controlled by means of an external stimulus, i.e., temperature, light, pressure, solvent interactions, or electric field.[38,39] This switching behavior makes them a target for Spintronics because the high-spin magnetic state usually presents higher conductance than the diamagnetic low-spin state.[12,40−46] The difference in the transport properties between the two states is due to the change in the electron configuration; the structural changes (larger metal−ligand bond distances in the high-spin state) play a minor role.[40,41]

In this study, we combine all of the above ingredients to design a single-molecule electrical wire that exhibits room-temperature conductance modulation of several orders of magnitude through spin-dependent transport. The junction is built by bridging individual Fe^{II} SCO complexes with high- and low-spin states between a gold electrode and a magnetically polarized nickel electrode. This is a fundamental difference from other experiments mentioned above that use two magnetic electrodes. The Fe^{II} complexes were designed with two axial −SCN (or −SeCN) chemical groups that served as the metal−molecule anchoring points (Figure 1).[47,48] Transport experiments with the high-spin complex show a single-molecule conductance change of at least 100-fold under opposite Ni magnetic polarization conditions. This large magnetoresistance switching is achieved at a near-zero bias voltage, which implies the use of very small currents and low power consumption. This change in conductance is observed when the electrons are injected from the gold to the magnetic nickel electrode, and the nickel electrode is magnetically polarized in opposite directions along the junction main axis. Our theoretical model suggests that the observed conductance change is the combined result of three consecutive stages. First, spin selection occurs at the molecule−gold interface as a result of new hybridized spin-polarized states. Second, the spin-polarized current generated at such interface by spin−orbit coupling (SOC) is enhanced by the high-spin $S = 2$ Fe^{II} complex that favors the transport of minority spin (α-up) carriers.[40] And third, the direction of the nickel magnetic polarization controls the final device conductance because the transport of minority spin carriers is also more efficient in the magnetically polarized tip.[49] The proposed model is supported by two control experiments: (i) the gold substrate is replaced by a copper one, which minimizes the spin surface effects due to the lack of large spin−orbit contributions, thereby canceling the first stage, and (ii) the paramagnetic high-spin complex is substituted by a homologous diamagnetic low-spin $S = 0$ Fe^{II} complex, whose molecule/metal interface cannot induce spin polarization in the carriers, thus eliminating the second stage of the mechanism.

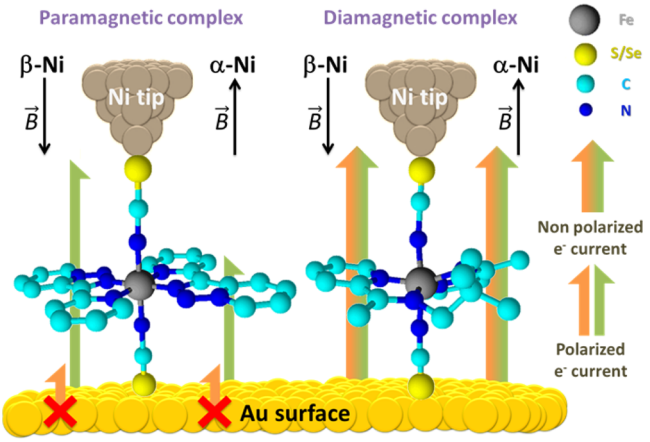

Figure 1. Schematic representation of the single-molecule junctions studied under two opposite Ni magnetic polarizations (labeled α and β). The paramagnetic [Fe(tzpy)$_2$(NCS)$_2$] complex shows a high conductance switching which depend on the Ni tip spin polarizations (see arrows), while the transport in the diamagnetic [FeL^A(NCS)$_2$] complex remains invariable.

Results and Discussion. *Single-Molecule Transport in Ambient Conditions.* Single-molecule conductance experiments under different Ni magnetic polarizations (Figure 1) were conducted on high-spin [Fe(tzpy)$_2$(NCS)$_2$] and [Fe(tzpy)$_2$(NCSe)$_2$][47] single-molecule contacts under ambient conditions using an STM break-junction approach.[15] Briefly, a freshly cut Ni tip was magnetically polarized ex situ by placing it in close proximity to a 1 T NdFeB magnet for a period of 2 h. After the magnetization, the Ni tip was placed into the STM tip

DOI: 10.1021/acs.nanolett.5b03571
Nano Lett. XXXX, XXX, XXX−XXX

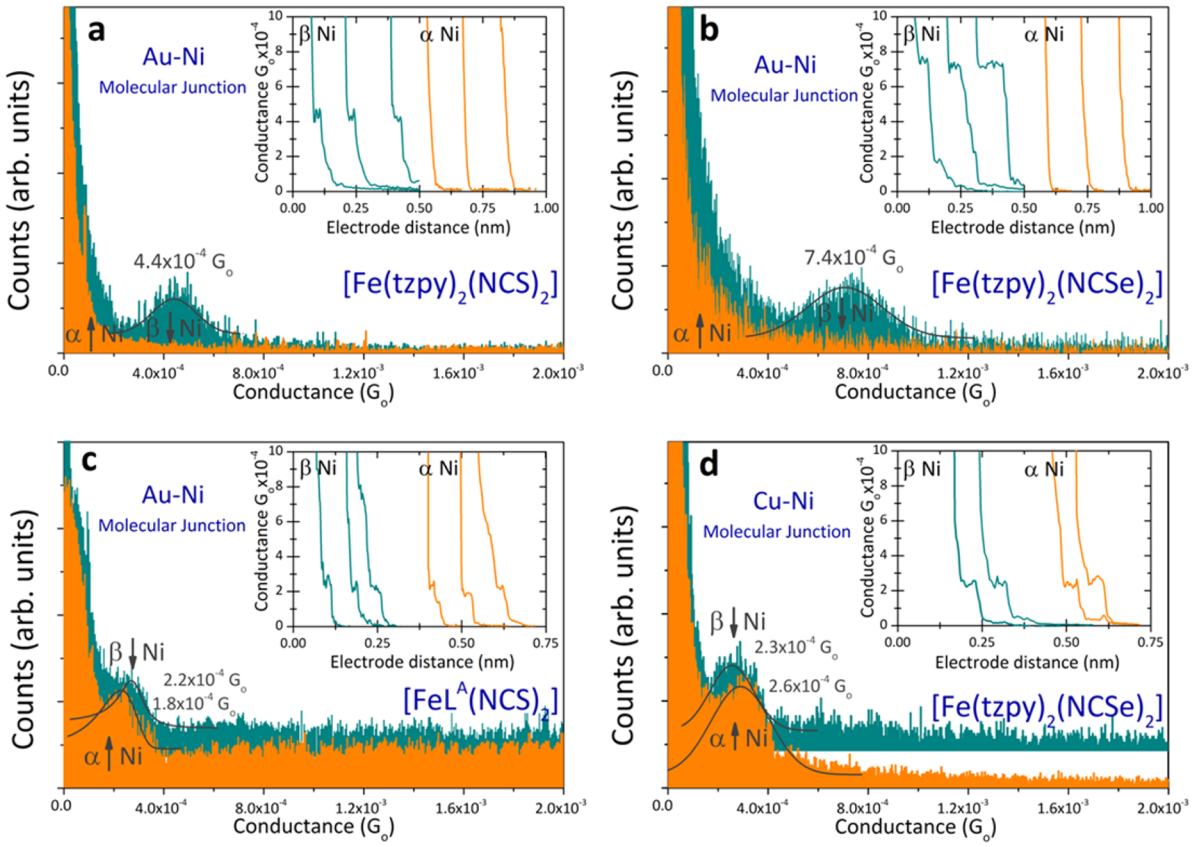

Figure 2. Conductance histograms for the single-molecule transport of Fe^{II} complexes under ambient conditions: (a) paramagnetic $[Fe(tzpy)_2(NCS)_2]$, (b) paramagnetic $[Fe(tzpy)_2(NCSe)_2]$, and (c) diamagnetic $[FeL^A(NCS)_2]$ complexes obtained with Au and both α-up polarized (orange) and β-down polarized (green) Ni electrodes. (d) Single-molecule conductance histograms for the $[Fe(tzpy)_2(NCSe)_2]$ complex obtained with Cu and both α-up polarized (orange) and β-down polarized (green) Ni electrodes. The two histograms have been vertically offset for clarity. All conductance values have been extracted from Gaussian fits of the peaks. Insets show representative current versus pulling traces used to build the conductance histograms for the α-up polarized (orange) and the β-down polarized (green) Ni electrodes. The applied bias was set to −10 mV.

holder. To avoid Ni oxidation during the magnetization stage, the Ni tip was kept under anaerobic conditions (see experimental details in Supporting Information (SI) sections 2.1 and 2.2). The magnitude and direction of the magnetic polarization of the Ni tip were characterized before and after the STM break-junction experiment using SQUID magnetometry to ensure that the Ni magnetization persisted over the entire time frame of the experiments (see SI section 2.3). The magnetized STM Ni probe was then driven toward the surface and pulled back again in successive cycles, using a 2-point feedback loop on the tunneling current flowing between the two electrodes under a constant bias voltage.[15,50]

Some representative current traces obtained during the pulling stage of the above successive cycles are shown in the insets of Figures 2a,b for the compounds in the high-spin state, $[Fe(tzpy)_2(NCS)_2]$ and $[Fe(tzpy)_2(NCSe)_2]$, respectively. When a molecule bridges between the two electrodes, a plateau appears in the current trace at the specific molecular conductance.[15,50] The −SCN group for molecular anchor purposes has been previously demonstrated in single-molecule contacts.[51] The absence of other exposed interacting groups in these compounds as well as the single plateau features in the decay curves[52,53] suggests the axial −S(Se)CN as the only anchoring points. In order to study spin-dependent transport across the single-molecule junctions, the conductance measurements were performed by magnetically polarizing the Ni electrode in the two opposite directions perpendicular to the surface (insets of Figure 2a,b). The α and β labels correspond to the magnetic polarization of the Ni electrode pointing upward and downward, respectively, from the SQUID characterization (SI section 2.3).

Two different charge transport behaviors are observed for the junction of the high spin Fe^{II} complex when the Ni electrode is magnetically polarized along either the α-up or the β-down directions and the electrons are injected from the Au to the Ni electrode (see Figure 1, left panel). When the Ni electrode is in the β-down polarization, both compounds, $[Fe(tzpy)_2(NCS)_2]$ and $[Fe(tzpy)_2(NCSe)_2]$, display current plateaus in the individual traces around characteristic conductance values (green curves in Figure 2a,b insets). Hundreds of these individual traces are accumulated into the corresponding conductance histogram where the peak maxima represent the most probable conductance values of the single-molecule contact (green histograms in Figure 2a,b). The $[Fe(tzpy)_2(NCSe)_2]$ displays a conductance of $7.4 \times 10^{-4}G_0$, roughly twice that of the $[Fe(tzpy)_2(NCS)_2]$, $4.4 \times 10^{-4}G_0$, which indicates higher electrical coupling in the former. This stronger Au−SeCN affinity also results in a longer average plateau length of 0.09 nm compared to 0.04 nm obtained for the SCN derivative (see SI section 4.5). These results also suggest that the molecules are anchored to the electrodes through Au−SCN/SeCN and Ni−SCN/SeCN bonds on each

DOI: 10.1021/acs.nanolett.5b03571
Nano Lett. XXXX, XXX, XXX−XXX

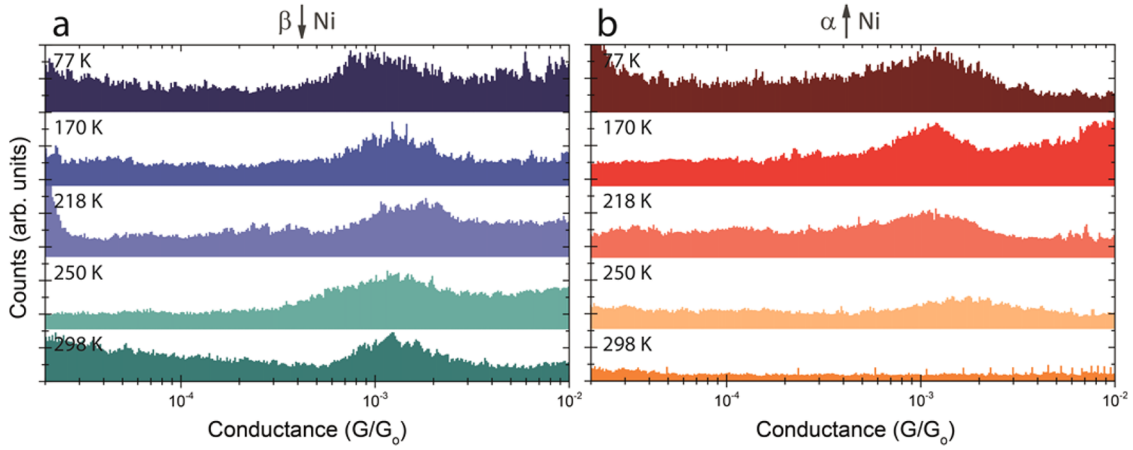

Figure 3. Temperature-dependent conductance histograms for the paramagnetic $[Fe(tzpy)_2(NCSe)_2]$ compound in vacuum under β-down (a) and α-up (b) Ni magnetic polarizations. The histograms have been vertically offset for clarity. The applied bias was set to −10 mV.

side of the junction, respectively. In contrast, no current plateaus were observed in the individual pulling traces for the α-up polarized Ni electrodes for either compound (orange curves in Figure 2a,b insets). The single-molecule conductance is in this case below the detection limit of our current amplifiers ($<10^{-6}G_0$, see orange histograms in Figure 2a,b). Note that single-molecule conductance switching is not observed when nonpolarized Ni electrodes are employed (see SI sections 4.3 and 4.4), where both molecules displays similar conductances.

To corroborate the role of the paramagnetic molecule in the observed spin-dependent transport experiment, single-molecule transport was also studied in a homologous diamagnetic low-spin $[FeL^A(NCS)_2]$ (L^A = *N*,*N*′-bis(1-pyridin-2-ylethylidene)-2,2-dimethylpropane-1,3-diamine) compound[52] (Figure 1). Similar conductance values were obtained under both α-up and β-down Ni magnetic polarizations (see Figure 2c), thus confirming that the spin-dependent conductance in the single-molecule contact stems from the paramagnetic nature of the compound, and that the formation of the single-molecule bridge is not affected by the magnetic polarization of the Ni electrode. Direct comparison of the single-molecule transport results in Figure 2 suggests a strong spin-dependent conductance switching for the high-spin Fe^{II} junction, i.e., the conductance of the paramagnetic single-molecule wire is suppressed in one of the Ni magnetic polarization directions. If a Cu substrate is used instead of Au, the observed spin-dependent transport for the $[Fe(tzpy)_2(NCSe)_2]$ compound is also suppressed (see Figure 2d).

Considering the small applied bias, the lack of magneto-resistance when the electrons are injected into the molecule from the spin polarized nickel electrode (see SI section 4.6, Figure S14) suggests that the spin polarized character of the current coming from the tip is responsible for the magneto-resistance suppression. In this scenario, magnetoresistance would be suppressed if the polarized current could modify the molecule's magnetic moment when both are antialigned. Transport in this case is due to minority carriers in the Ni tip with a spin opposite to the molecule, which is aligned with the magnetization of the tip. Spin-transfer torque mechanisms, well established in layered systems, could apply to our molecular bridge if, for instance, one assumes the magnetic interaction between the exchange field at the molecule and at the magnetization of the transient electron.[54−56] Further studies are needed to clarify such mechanism.

Temperature-Dependent Single-Molecule Transport. To further demonstrate that the observed single-molecule spin-dependent transport depends on the paramagnetic properties of the molecule, we also examined the conductance switching of the single-molecule Fe^{II} complex $[Fe(tzpy)_2(NCSe)_2]$ device as a function of temperature. This compound transits from a high-spin state at room temperature ($t_{2g}^4e_g^2$), to a low-spin state below ∼250 K, so the current blockage under α-up Ni electrode magnetization should not be observed at low temperatures. To test this hypothesis, single-molecule wires were characterized in a vacuum STM break-junction system (see experimental details in SI section 4.9). Figure 3a,b shows comparable conductance histograms for the two β-down and α-up Ni electrode magnetic polarizations respectively as a function of the sample temperature. At low temperatures (well below the spin transition at ∼250 K), a single-molecule feature is observed, which is independent of the magnetic polarization (α-up, β-down) of the Ni tip, comparable to what we observe in the low-spin $[FeL^A(NCS)_2]$ at room temperature (Figure 2c). The observed ∼5-fold difference in conductance between both low-spin scenarios ($[FeL^A(NCS)_2]$ at room temperature and $[Fe(tzpy)_2(NCSe)_2]$ at low temperature) can be ascribed to the different ligand field for the Fe center in both complexes as well as the different anchoring group, going from the more −SCN to the less resistive −SeCN. In the α-up case, a monotonic decrease of the peak height in the single-molecule conductance histograms is observed as the temperature crosses the transition point (∼250 K) of the spin-crossover compound from the low to the high electronic spin configuration (see SI section 3.2). At temperatures close to room temperature, the conductance histogram displays no maximum under this α-up Ni electrode polarization in analogy to the one presented in Figure 2b (orange) for the same compound measured under ambient conditions. Likewise, a single-molecule feature is observed at 298 K under β-down Ni polarization (Figure 3a), which is similar to the measurements under same polarization in ambient conditions (Figure 2b). The slight <2-fold observed difference in conductance is likely due to the different environments (vacuum versus organic medium, see Experimental Section) Note that the conductance values for the low-spin and the high-spin molecular wires are statistically indistinguishable, and they are also similar, within the experimental error, to both β-down and nonpolarized Ni electrodes. The same results were also found for the

DOI: 10.1021/acs.nanolett.5b03571
Nano Lett. XXXX, XXX, XXX−XXX

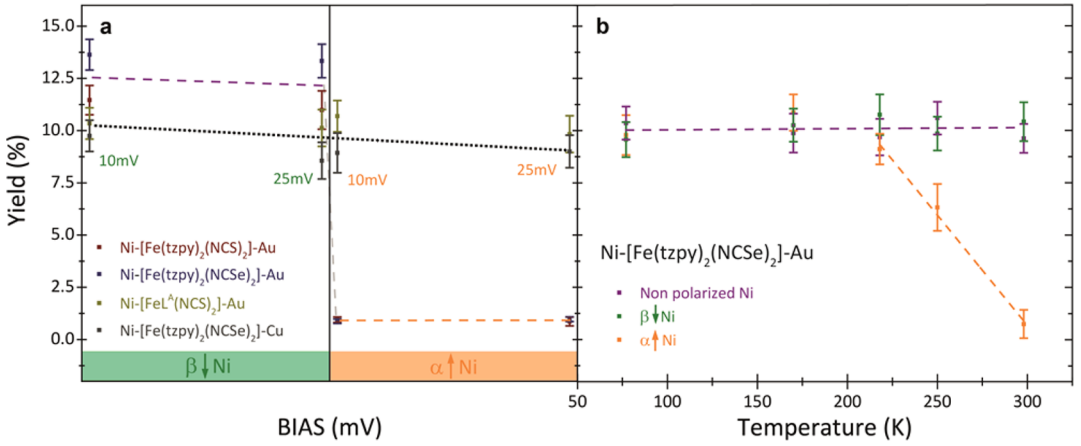

Figure 4. Yield values (%) of current plateau appearance in single-molecule experiments. The β-down and α-up Ni polarizations are in green and orange, respectively. (a) The three different complexes $[Fe(tzpy)_2(NCS)_2]$, $[Fe(tzpy)_2(NCSe)_2]$, and diamagnetic $[FeL^A(NCS)_2]$ are showed in red, blue, and yellow, respectively. Transport measurements with the Cu electrode are showed in gray. Different points correspond to different bias voltages and the error bars denote the standard deviation from different experiments. (b) The paramagnetic $[Fe(tzpy)_2(NCSe)_2]$ was also measured as a function of temperature under both Ni polarizations showing the spin transition under the α-up Ni polarization. The dotted lines connect the average points as a visual guide.

experiments performed under ambient conditions (see Figures 2b and SI12). These observations suggest that one of the spin-polarized channels (the α channel) at the molecule/Au interface fundamentally dominates the conducting state of the paramagnetic spin-crossover molecular junction in all cases.

The results in Figures 2 and 3 can be also analyzed in terms of the frequency of the observed single-molecule events in the experimental curves, named molecular junction yield (%). Because the spin-polarization effect can be also subjected to statistical variations even under a fixed Ni magnetic polarization (not every electron crossing the junction will be spin-polarized), the single-molecule yield will bring a more statistically meaningful picture to the observed spin-dependent single-molecule conductance behavior. The yield in single-molecule experiments represents the percentage of individual traces that display current plateaus over the total number of curves acquired. When this number is low (below 1%), no peaks in the conductance histogram are observed, meaning that the measured conductance of any formed molecular junction between the electrodes is statistically outside the experimentally accessible current range. Figure 4a summarizes the experimental yield of the single-molecule transport experiments in ambient conditions for all studied Fe compounds under the two Ni magnetic polarizations.

All three compounds, the paramagnetic $[Fe(tzpy)_2(NCS)_2]$ and $[Fe(tzpy)_2(NCSe)_2]$ as well as the diamagnetic $[Fe-L^A(NCS)_2]$, present yields above 10% for the junctions formed between the β-polarized Ni and Au electrodes, with the yield usually being larger for the $[Fe(tzpy)_2(NCSe)_2]$ complex due to its stronger binding affinity. Yields between 5% and 20% are currently obtained in well-established single-molecule contacts with dithiolated backbones (see SI section 4.7).[57,58] In contrast, when the Ni polarization is inverted, the yield for the two paramagnetic compounds drop to values below 1%, whereas the yield for the diamagnetic complex remains constant. A comparable behavior of the yield is observed as a function of the sample temperature (Figure 4b). With the α-Ni polarization, the measured yield changes from the standard values (>10%) to low values (<1%) when the increasing temperature crosses the transition temperature for this SCO compound (SI section 3.2). The observed transition occurs over a fairly wide temperature range around the bulk transition temperature, in agreement with recent spectroscopic studies of similar SCO compounds on a 2D Au nanoparticles film.[47,59] Such shallow transition is the reflection of the progressive change of the high-spin to low-spin population ratio as the temperature crosses the transition point. All together, the above result demonstrates the transition of a single-molecule wire from a high-spin (room temperature) to a low-spin state (low temperature), displaying large room temperature conductance switching (<10 000%).

Theoretical Calculations. We have considered two possible scenarios in order to explain the magnetoresistance effect when the transport is going from the Au surface to the Ni tip. The first one considers that the magnetic anisotropy of the molecule−surface ensemble is large enough to keep the molecular spin aligned in a preferent direction, and, consequently, it will result in a different transport of α and β electrons through the molecule. Alternatively, the second scenario assumes that the spin of the molecule remains aligned with the magnetization of the nickel tip, and it is the interaction of the molecular levels with some spin polarized bands of the gold surface that induce the observed spin filter behavior.

In order to check the magnitude of the magnetic anisotropy of the system, we performed theoretical CASSCF calculations using an accurate procedure to include spin−orbit effects (RASSI method, see SI section 5.2). Single-determinant methods, such as those based on DFT, fail for systems with large magnetic anisotropy. CASSCF multireference approach properly introduces the spin−orbit effect, but it is limited to nonperiodic small systems. The calculation of the isolated high spin Fe^{II} complex and such molecule deposited on small Au_4 cluster to model the structure gives in both cases moderate magnetic anisotropy (barriers around 20 K). This fact suggests the unlikeliness of the first scenario that would require a very high magnetic anisotropy to explain the observed magnetoresistance effect at room temperature.

To understand the origin of the observed spin-polarization differences in the electron currents traversing the molecular junctions and address the interplay between the changing molecule's magnetic moment (second scenario described above) and the surface states, we performed density functional theory (DFT) based calculations including SOC and modeled

DOI: 10.1021/acs.nanolett.5b03571
Nano Lett. XXXX, XXX, XXX−XXX

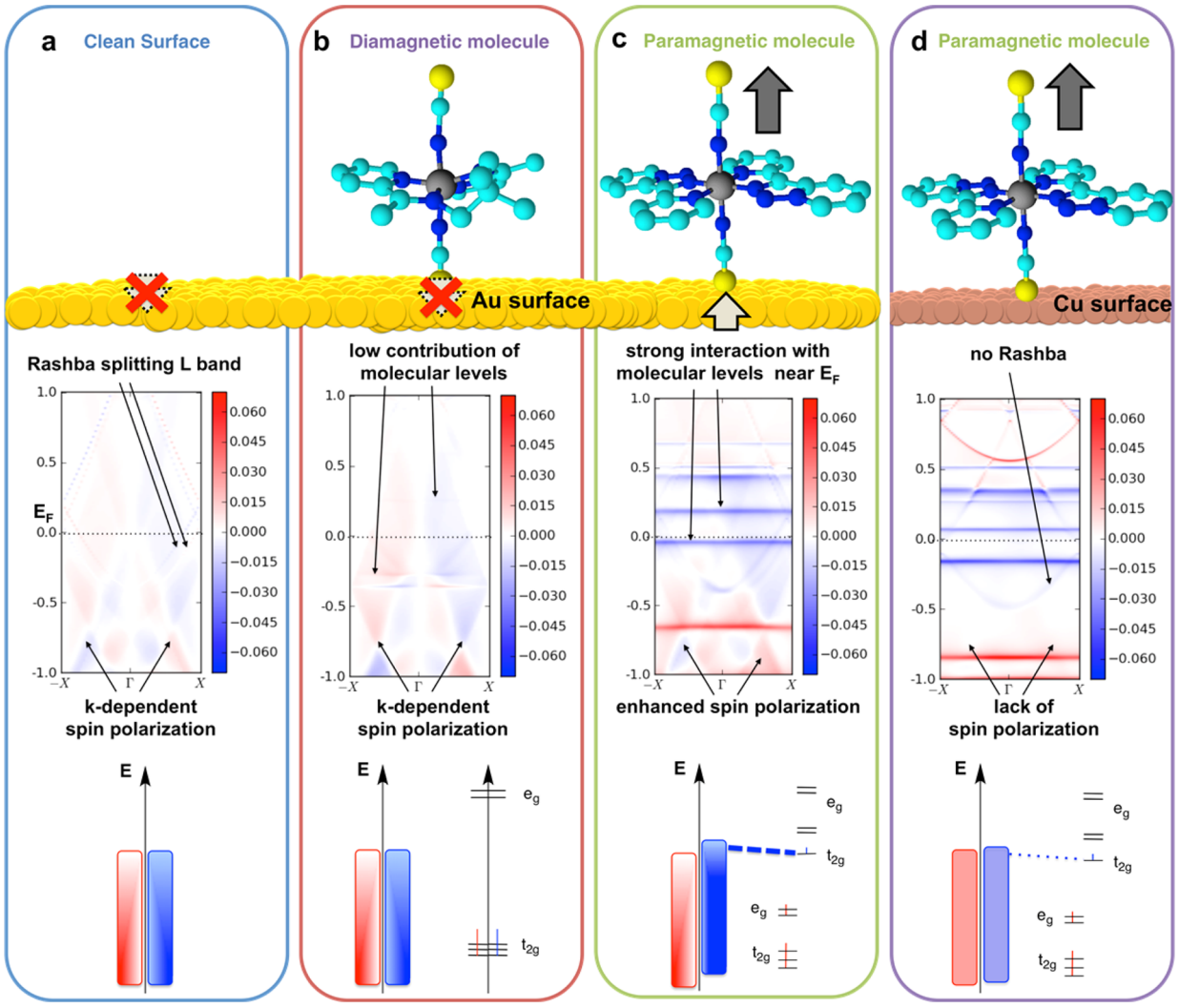

Figure 5. Calculated out of plane spin texture for the clean and covered Au(111) surface: DFT calculated logarithm of the z component of the magnetization for the DOS(α)-DOS(β) difference (central panel) and a schematic DOS representation (bottom panel) for the clean and covered Au(111) surfaces. The usual splitting of L-band and a k-dependent spin-polarization (Rashba effect) is found in the DFT calculations for the gold surface systems (a–c), also indicated with a nonuniform filling in the schematic DOS of the surface bands as opposed to the copper surface. (d) Symmetric spin-polarized levels will vanish for panels a and b when summing over the Brillouin zone. Horizontal lines correspond to the hybridized molecular levels for the high-spin Fe^{II} complex adsorbed to the electrode surface (c,d). Moreover, relative high spin polarization of the gold surface (k-dependent spin polarization) occurs when a high-spin Fe^{II} complex is strongly adsorbed through its single β t_{2g} electron (c). This effect is small when absorbed on the copper surface (d).

the surfaces as true semi-infinite systems (see SI section 5.1). We considered the four different cases employed in the nanoscale transport experiments (Figure 5a–d): (i) a clean Au(111) surface; (ii) a diamagnetic $[FeL^{A}(NCS)_2]$ molecule deposited on the same gold surface, and (iii) the paramagnetic $[Fe(tzpy)_2(NCS)_2]$ complex deposited on both Au(111) and (iv) Cu(111) surfaces. k-Resolved magnetization maps along the surface normal, $S\_z(E,k)$, projected on the surface atoms attached to the anchoring S are presented in the Figure 5a-d central panel. As expected from a strong SOC, the characteristic L-band splitting and a rich k-dependent spin texture is obtained for all gold systems, while absent in the copper surface (see also Figure S17), confirming that the Rashba effect is accurately taken into account in our calculations by the inclusion of the large spin–orbit contributions of the gold surface.[60,61] In the presence of absorbed paramagnetic molecule (Figure 5c-d), up to five minority spin molecular levels (horizontal blue lines) hybridize with the metal and become transport-dominant around the Fermi level.

In Figure 5a–c, we present the density of states (DOS, majority-α colored in red and minority-β in blue) of the studied interfaces (see calculations in SI section 5). Indeed, for the nonmagnetic cases (Figure 5a,b), the DOS of the gold electrodes has a k-dependent spin polarization due to the large spin–orbit effects (red versus blue regions in Figure 5), but cancels out when summing over the Brillouin zone (strong symmetry in the k-dependent spin-polarized DOS in Figures 5a,b). For the paramagnetic molecule absorbed on a Au surface (Figure 5c), there is a fairly strong interaction of the single spin molecular levels with the metal energy levels around the Fermi energy. It is worth noting the small hybridization of the molecular orbitals in the $[FeL^{A}(NCS)_2]$ complex with the surface due to the nonbonding nature of the t_{2g} orbitals (see Figure 5b and also Figure S17b). The paramagnetic $[Fe(tzpy)_2(NCS)_2]$ complex induces a small spin delocalization[62]

DOI: 10.1021/acs.nanolett.5b03571
Nano Lett. XXXX, XXX, XXX–XXX

(same sign as that of the molecule) in the three gold atoms directly bonded to the anchoring sulfur atom (0.004 e^- with same sign as that of the molecule, Figure 5c), which is not fully compensated by an opposite spin density of 0.002 e^- found for the rest of the gold surface layer (see Table S1). The results for the Cu/paramagnetic molecule scenario reveal a very low increase of the spin polarization of the surface (Figure 5d) after the interaction with the high spin Fe^{II} complex, in contrast to the Au/paramagnetic molecule case (Figure 5c).

The above theoretical analysis reveals the key ingredients that determine the spin-dependent transport measured in the single-molecule experiments (Figure 2); the effective SOC and its interplay with the induced spin polarization at the metallic surface is responsible for the spin-polarization of the electrons traversing the Au electrode/paramagnetic compound interface. This spin-polarized current crosses the single-molecule bridge and translates into different conductances values depending on the particular α- or β-magnetization of the Ni electrode, and results in the observed overall conductance switching of the single-molecule device.

The experimental results are also in agreement with previous DFT transport calculations showing a large preference for the minority carriers in the high-spin d^6 Fe^{II} complexes, i.e., $[Fe(tzpy)_2(NCS)_2]$ and $[Fe(tzpy)_2(NCSe)_2]$ S = 2 complexes.[40] Assuming five α and one β electrons, the highest occupied (HOMO) and lowest unoccupied (LUMO) β-molecular orbital levels lie very close to the electrode Fermi levels (Figure 5c) and they are responsible for the spin-polarized transport. In addition, there is an enhancement of the spin polarization of the gold surface due to the interaction with the magnetic molecule (Figure 5c). This spin polarization of the gold levels results in a favorable interaction with one of the two molecular channels that explains the observed conductance change as a function of the Ni electrode magnetization direction. The t_{2g} and e_g levels for the diamagnetic $[FeL^A(NCS)_2]$ complex are identically occupied, therefore, α and β channels are equivalent and, consequently, no spin-dependent transport is observed. The spin-polarized Au electrode/paramagnetic molecule interface (also present in carbon nanotube based devices)[22−24] is the critical effect that allows the spin-polarized current, and it is both experimentally and theoretically corroborated by the lack of such an effect in the homologous copper device (Figures 2d and 5d).

It is noted here that the proposed calculation corresponds to an analysis of the electronic structure of the molecule−surface interface aimed for the identification of key points that consistently explain the observed dependence of the current on (i) the tip magnetization direction, (ii) the material of the electrode (Au or Cu), and (iii) the spin state of the bridging molecule. The accurate calculation of the transmission function would correspond to the bias-dependent current that is beyond the two-channel model and out of reach for current computational methodologies.

Experimental Section. Relevant methodological details are included in this section. For further details, an extended version is available in the SI file linked to this work.

Surface Preparation. A Au(111) single crystal (Matek, Germany) was surface-functionalized with either $[Fe(tzpy)_2(NCS)_2]$ or $[Fe(tzpy)_2(NCSe)_2]$ compounds (basic information on the synthesis and characterization can be found in the SI sections 3.1 and 3.2)[47] by immersion in a μM ethanolic solution of the target compound for periods longer than 6 h. XPS measurements of the resulting SAMs confirmed the presence of the Fe complex on the Au surface as well as the formation of an Au−S/Au-Se bond (see SI sections 1.2). In order to avoid formation of molecular aggregates in solution during the absorption of the target compounds onto the Au surface, we used concentrations within the low Lambert−Beer range (see SI section 1.1). The last point is determinant to get clean single-molecule transport results.

Conductance Measurements. An STM-BJ method[15] was employed to build and characterize charge transport through single-molecule wires built with the different Fe^{II} complexes studied in this work. The two biased (−10 mV) electrodes in the molecular junction, a Au(111) single crystal (99.99% Matek, Germany) and a mechanically cut polycrystalline Ni wire (99.99%, Godfellow, UK) were used as the support and the STM top electrodes, respectively. In a regular STM-BJ experiment (see manuscript), the Ni tip was repeatedly driven onto the Au surface in the presence of molecules (unless indicated), while simultaneously monitoring the current flowing between them. Several thousands (∼5000) retraction curves were then stored and used to build the conductance histogram of the single-molecule device. Because not every curve displayed plateau features corresponding to the molecular quantum conductance of the single-molecule bridge, we designed an automatic algorithm that identifies and selects curves containing such single-molecule features. The exact same selection criteria were applied throughout all measured series. To avoid the Ni wire oxidation under ambient conditions, the prepared Ni electrode was magnetically polarized and stored under in anaerobic conditions before use. All experiments were conducted in an organic solvent mesitylene (unless otherwise indicated) with very low oxygen and water solubility. The Ni tip oxidation was monitored during use by ex situ SEM-EDS electron microscopy (see SI section 2.2).

Computational Calculations. DFT calculations were performed with the GREEN code[63] and its interface to the DFT-based SIESTA package[64] including the recently implemented fully relativistic pseudopotential (PP) formalism, in order to account for spin−orbit coupling (SOC) contributions[65] (see SI section 5.1 for more details). CASSCF-RASSI calculations were conducted to determine the magnetic anisotropy of the Fe^{II} complex and the molecule deposited on Au_4 cluster (see SI section 5.2 for more details).

Conclusion. We present an example of large room temperature conductance switching based on spin-dependent transport in a single-molecule device that results upon the strong interaction of a paramagnetic molecule with heavy-metal surface atoms. This finding represents a new form of generating large magnetoresistance effects in a single-molecule device in the absence of an applied external magnetic field. Our qualitative theoretical model sets the key ingredients to account for the observed large spin-dependent conductance switching in the single-molecule device: (i) Engineering a hybrid electrode/molecule interface that results in spin-polarized states. This spinterface is responsible for the polarization of the current flowing through the single-molecule contact. (ii) Selecting a paramagnetic molecule with appropriate electronic structure, as the high-spin Fe^{II} complexes, to favor transport through one of the spin channels. (iii) Using a spin-polarized ferromagnetic electrode on one side of the single-molecule junction that acts as the spin-polarized electron *drain*. Imposing different directions of the top electrode's magnetic polarization then controls the observed magnetoresistance.

DOI: 10.1021/acs.nanolett.5b03571
Nano Lett. XXXX, XXX, XXX−XXX

These experiments demonstrate the crucial role that the molecule−surface magnetic interactions, the spinterface,[66] have on the design of the next generation of nanoscale spintronic devices and set the basis for future design of nanoscale magnetic molecular circuits.

■ ASSOCIATED CONTENT

Supporting Information

The Supporting Information is available free of charge on the ACS Publications website at DOI: 10.1021/acs.nanolett.5b03571.

Sample characterization (section S1), Ni electrodes characterization (section S2), preparation and magnetic characterization of the molecular system SAMs (section S3), single-molecule transport measurements (section S4), and computational details (section S5) (PDF)

■ AUTHOR INFORMATION

Corresponding Authors

*E-mail: isma_diez@ub.edu.
*E-mail: eliseo.ruiz@qi.ub.es.
*E-mail: jhihath@ucdavis.edu.

Notes

The authors declare no competing financial interest.

■ ACKNOWLEDGMENTS

This research was supported by the Spanish *Ministerio de Economía y Competitividad* (Grants CTQ2012-36090, CTQ2011-23862-C02-01, MAT2013-47878-C2-R and CTQ2010-18414 and *Generalitat Valenciana* (GVPROMETEO2012-049) as well as the United States National Science Foundation (J.H. and H.L. ECCS-1231915). D.A. thanks *Conicyt-Chile* for a predoctoral fellowship. A.C.A. and Z.A.-C. thank the Spanish *Ministerio de Educación, Cultura y Deporte* for graduate FPU fellowships. I.D.-P. thanks the Ramon y Cajal program (MINECO) and the EU Reintegration Grant (FP7-PEOPLE-2010-RG-277182) for financial support. E.R. thanks Generalitat de Catalunya for an ICREA academia award. The authors acknowledge the general facilities of the University of Barcelona (CCiT-UB) and the computer resources, technical expertise, and assistance provided by the Barcelona Supercomputing Centre.

■ REFERENCES

(1) Wolf, S. A.; Awschalom, D. D.; Buhrman, R. A.; Daughton, J. M.; von Molnar, S.; Roukes, M. L.; Chtchelkanova, A. Y.; Treger, D. M. *Science* **2001**, *294*, 1488.
(2) Zutic, I.; Fabian, J.; Das Sarma, S. *Rev. Mod. Phys.* **2004**, *76*, 323.
(3) Sinova, J.; Žutić, I. *Nat. Mater.* **2012**, *11*, 368.
(4) Sanvito, S. *Chem. Soc. Rev.* **2011**, *40*, 3336.
(5) Schmaus, S.; Bagrets, A.; Nahas, Y.; Yamada, T. K.; Bork, A.; Bowen, M.; Beaurepaire, E.; Evers, F.; Wulfhekel, W. *Nat. Nanotechnol.* **2011**, *6*, 185.
(6) Schwobel, J.; Fu, Y. S.; Brede, J.; Dilullo, A.; Hoffmann, G.; Klyatskaya, S.; Ruben, M.; Wiesendanger, R. *Nat. Commun.* **2012**, *3*, 953.
(7) Wiesendanger, R. *Rev. Mod. Phys.* **2009**, *81*, 1495.
(8) Mugarza, A.; Krull, C.; Robles, R.; Stepanow, S.; Ceballos, G.; Gambardella, P. *Nat. Commun.* **2011**, *2*, 490.
(9) Krull, C.; Robles, R.; Mugarza, A.; Gambardella, P. *Nat. Mater.* **2013**, *12*, 337.
(10) Alam, M. S.; Stocker, M.; Gieb, K.; Müller, P.; Haryono, M.; Student, K.; Grohmann, A. *Angew. Chem., Int. Ed.* **2010**, *49*, 1159.
(11) Mugarza, A.; Robles, R.; Krull, C.; Korytár, R.; Lorente, N.; Gambardella, P. *Phys. Rev. B: Condens. Matter Mater. Phys.* **2012**, *85*, 155437.
(12) Miyamachi, T.; Gruber, M.; Davesne, V.; Bowen, M.; Boukari, S.; Joly, L.; Scheurer, F.; Rogez, G.; Yamada, T. K.; Ohresser, P.; Beaurepaire, E.; Wulfhekel, W. *Nat. Commun.* **2012**, *3*, 938.
(13) Ramachandran, G. K.; Hopson, T. J.; Rawlett, A. M.; Nagahara, L. A.; Primak, A.; Lindsay, S. M. *Science* **2003**, *300*, 1413.
(14) Reed, M. A.; Zhou, C.; Muller, C. J.; Burgin, T. P.; Tour, J. M. *Science* **1997**, *278*, 252.
(15) Xu, B.; Tao, N. J. *Science* **2003**, *301*, 1221.
(16) Heersche, H. B.; de Groot, Z.; Folk, J. A.; van der Zant, H. S. J.; Romeike, C.; Wegewijs, M. R.; Zobbi, L.; Barreca, D.; Tondello, E.; Cornia, A. *Phys. Rev. Lett.* **2006**, *96*, 206801.
(17) Parks, J. J.; Champagne, A. R.; Costi, T. A.; Shum, W. W.; Pasupathy, A. N.; Neuscamman, E.; Flores-Torres, S.; Cornaglia, P. S.; Aligia, A. A.; Balseiro, C. A.; Chan, G. K.-L.; Abruña, H. D.; Ralph, D. C. *Science* **2010**, *328*, 1370.
(18) Burzurí, E.; Zyazin, A. S.; Cornia, A.; van der Zant, H. S. J. *Phys. Rev. Lett.* **2012**, *109*, 147203.
(19) Bagrets, A.; Schmaus, S.; Jaafar, A.; Kramczynski, D.; Yamada, T. K.; Alouani, M.; Wulfhekel, W.; Evers, F. *Nano Lett.* **2012**, *12*, 5131.
(20) Li, J.-J.; Bai, M.-L.; Chen, Z.-B.; Zhou, X.-S.; Shi, Z.; Zhang, M.; Ding, S.-Y.; Hou, S.-M.; Schwarzacher, W.; Nichols, R. J.; Mao, B.-W. *J. Am. Chem. Soc.* **2015**, *137*, 5923.
(21) Mannini, M.; Pineider, F.; Sainctavit, P.; Danieli, C.; Otero, E.; Sciancalepore, C.; Talarico, A. M.; Arrio, M.-A.; Cornia, A.; Gatteschi, D.; Sessoli, R. *Nat. Mater.* **2009**, *8*, 194.
(22) Urdampilleta, M.; Klyatskaya, S.; Cleuziou, J. P.; Ruben, M.; Wernsdorfer, W. *Nat. Mater.* **2011**, *10*, 502.
(23) Vincent, R.; Klyatskaya, S.; Ruben, M.; Wernsdorfer, W.; Balestro, F. *Nature* **2012**, *488*, 357.
(24) Ganzhorn, M.; Klyatskaya, S.; Ruben, M.; Wernsdorfer, W. *Nat. Nanotechnol.* **2013**, *8*, 165.
(25) Komeda, T.; Isshiki, H.; Liu, J.; Zhang, Y.-F.; Lorente, N.; Katoh, K.; Breedlove, B. K.; Yamashita, M. *Nat. Commun.* **2011**, *2*, 217.
(26) Lodi Rizzini, A.; Krull, C.; Balashov, T.; Kavich, J. J.; Mugarza, A.; Miedema, P. S.; Thakur, P. K.; Sessi, V.; Klyatskaya, S.; Ruben, M.; Stepanow, S.; Gambardella, P. *Phys. Rev. Lett.* **2011**, *107*, 177205.
(27) Xie, Z.; Markus, T. Z.; Cohen, S. R.; Vager, Z.; Gutierrez, R.; Naaman, R. *Nano Lett.* **2011**, *11*, 4652.
(28) Yeganeh, S.; Ratner, M. A.; Medina, E.; Mujica, V. *J. Chem. Phys.* **2009**, *131*, 014707.
(29) Göhler, B.; Hamelbeck, V.; Markus, T. Z.; Kettner, M.; Hanne, G. F.; Vager, Z.; Naaman, R.; Zacharias, H. *Science* **2011**, *331*, 894.
(30) Carmeli, I.; Leitus, G.; Naaman, R.; Reich, S.; Vager, Z. *J. Chem. Phys.* **2003**, *118*, 10372.
(31) Naaman, R.; Vager, Z. *Phys. Chem. Chem. Phys.* **2006**, *8*, 2217.
(32) Vager, Z.; Naaman, R. *Chem. Phys.* **2002**, *281*, 305.
(33) Nealon, G. L.; Donnio, B.; Greget, R.; Kappler, J. P.; Terazzi, E.; Gallani, J. L. *Nanoscale* **2012**, *4*, 5244.
(34) Hernando, A.; Crespo, P.; Garcia, M. A.; Pinel, E. F.; de la Venta, J.; Fernandez, A.; Penades, S. *Phys. Rev. B: Condens. Matter Mater. Phys.* **2006**, *74*, 052403.
(35) Bychkov, Y. A.; Rashba, E. I. *J. Phys. C: Solid State Phys.* **1984**, *17*, 6039.
(36) Koga, T.; Nitta, J.; Takayanagi, H.; Datta, S. *Phys. Rev. Lett.* **2002**, *88*, 126601.
(37) Ting, D. Z. Y.; Cartoixa, X. *Appl. Phys. Lett.* **2002**, *81*, 4198.
(38) Halcrow, M. A. *Spin-Crossover Materials: Properties and Applications*; Wiley: Chichester, U.K., 2013.
(39) Ruiz, E. *Phys. Chem. Chem. Phys.* **2014**, *16*, 14.
(40) Aravena, D.; Ruiz, E. *J. Am. Chem. Soc.* **2012**, *134*, 777.
(41) Baadji, N.; Sanvito, S. *Phys. Rev. Lett.* **2012**, *108*, 217201.
(42) Martinho, P. N.; Rajnak, C.; Ruben, M. In *Spin-Crossover Materials: Properties and Applications*; John Wiley & Sons, Ltd: Chichester, U.K., 2013; p 375.
(43) Meded, V.; Bagrets, A.; Fink, K.; Chandrasekar, R.; Ruben, M.; Evers, F.; Bernand-Mantel, A.; Seldenthuis, J. S.; Beukman, A.; van der

DOI: 10.1021/acs.nanolett.5b03571
Nano Lett. XXXX, XXX, XXX−XXX

Zant, H. S. J. *Phys. Rev. B: Condens. Matter Mater. Phys.* **2011**, *83*, 245415.
(44) Wagner, S.; Kisslinger, F.; Ballmann, S.; Schramm, F.; Chandrasekar, R.; Bodenstein, T.; Fuhr, O.; Secker, D.; Fink, K.; Ruben, M.; Weber, H. B. *Nat. Nanotechnol.* **2013**, *8*, 575.
(45) Gopakumar, T. G.; Matino, F.; Naggert, H.; Bannwarth, A.; Tuczek, F.; Berndt, R. *Angew. Chem., Int. Ed.* **2012**, *51*, 6262.
(46) Prins, F.; Monrabal-Capilla, M.; Osorio, E. A.; Coronado, E.; van der Zant, H. S. J. *Adv. Mater.* **2011**, *23*, 1545.
(47) Niel, V.; Gaspar, A. B.; Munoz, M. C.; Abarca, B.; Ballesteros, R.; Real, J. A. *Inorg. Chem.* **2003**, *42*, 4782.
(48) Lissel, F.; Schwarz, F.; Blacque, O.; Riel, H.; Lörtscher, E.; Venkatesan, K.; Berke, H. *J. Am. Chem. Soc.* **2014**, *136*, 14560.
(49) Johnson, M. *Handbook of Spin Transport and Magnetism*; Chapman and Hall/CRC: Boca Raton, FL, 2011.
(50) Xia, J. L.; Diez-Perez, I.; Tao, N. J. *Nano Lett.* **2008**, *8*, 1960.
(51) Ko, C.-H.; Huang, M.-J.; Fu, M.-D.; Chen, C.-h. *J. Am. Chem. Soc.* **2010**, *132*, 756.
(52) Brefuel, N.; Vang, I.; Shova, S.; Dahan, F.; Costes, J. P.; Tuchagues, J. P. *Polyhedron* **2007**, *26*, 1745.
(53) Kiguchi, M.; Ohto, T.; Fujii, S.; Sugiyasu, K.; Nakajima, S.; Takeuchi, M.; Nakamura, H. *J. Am. Chem. Soc.* **2014**, *136*, 7327.
(54) Tserkovnyak, Y.; Brataas, A.; Bauer, G. E. W.; Halperin, B. I. *Rev. Mod. Phys.* **2005**, *77*, 1375.
(55) Haney, P. M.; et al. *Phys. Rev. B: Condens. Matter Mater. Phys.* **2007**, *76*, 024404.
(56) Jiang, L.; Liu, X.; Zhang, Z.; Wang, R. *Phys. Lett. A* **2014**, *378*, 426.
(57) Li; Hihath, J.; Chen, F.; Masuda, T.; Zang, L.; Tao. *J. Am. Chem. Soc.* **2007**, *129*, 11535.
(58) Hines, T.; Díez-Pérez, I.; Nakamura, H.; Shimazaki, T.; Asai, Y.; Tao, N. *J. Am. Chem. Soc.* **2013**, *135*, 3319.
(59) Devid, E. J.; Martinho, P. N.; Kamalakar, M. V.; Šalitroš, I.; Prendergast, Ú.; Dayen, J.-F.; Meded, V.; Lemma, T.; González-Prieto, R.; Evers, F.; Keyes, T. E.; Ruben, M.; Doudin, B.; van der Molen, S. J. *ACS Nano* **2015**, *9*, 4496.
(60) Mazzarello, R.; Corso, A. D.; Tosatti, E. *Surf. Sci.* **2008**, *602*, 893.
(61) Kosugi, T.; Miyake, T.; Ishibashi, S. *J. Phys. Soc. Jpn.* **2011**, *80*, 074713.
(62) Cano, J.; Ruiz, E.; Alvarez, S.; Verdaguer, M. *Comments Inorg. Chem.* **1998**, *20*, 27.
(63) Cerda, J.; Van Hove, M. A.; Sautet, P.; Salmeron, M. *Phys. Rev. B: Condens. Matter Mater. Phys.* **1997**, *56*, 15885.
(64) Soler, J. M.; Artacho, E.; Gale, J. D.; Garcia, A.; Junquera, J.; Ordejon, P.; Sanchez-Portal, D. *J. Phys.: Condens. Matter* **2002**, *14*, 2745.
(65) Cuadrado, R.; Cerda, J. I. *J. Phys.: Condens. Matter* **2012**, *24*, 086005.
(66) Sanvito, S. *Nat. Phys.* **2010**, *6*, 562.

DOI: 10.1021/acs.nanolett.5b03571
Nano Lett. XXXX, XXX, XXX−XXX